This is the peer-reviewed, final accepted version for American Mineralogist, published by the Mineralogical Society of America.
The published version is subject to change. Cite as Authors (Year) Title. American Mineralogist, in press.
DOI: https://doi.org/10.2138/am-2021-7853. http://www.minsocam.org/

Revision 1

Elasticity and high pressure behavior of $Mg_2Cr_2O_5$ and $CaTi_2O_4$-type phases of magnesiochromite and chromite

Sean R. Shieh[a,b*], Tauhid Belal Khan[a], Zhongying Mi[a], Mauritz van Zyl[a], Ricardo D. Rodriguez[a], Clemens Prescher[c], Vitali B. Prakapenka[c]

[a] Department of Earth Sciences, University of Western Ontario, London, Canada

[b] Department of Physics and Astronomy, University of Western Ontario, London, Canada

[c] Center for Advanced Radiation Sources, The University of Chicago, Chicago, USA

Abstract

In situ high-pressure and high-temperature X-ray diffraction studies on magnesiochromite, $MgCr_2O_4$ and a natural chromite, $(Mg,Fe)(Al,Cr)_2O_4$ using a laser-heated diamond anvil cell technique were performed at pressures to about 45 GPa. Our results on $MgCr_2O_4$ at ~15 GPa showed temperature-induced dissociation of $MgCr_2O_4$ to Cr_2O_3 + MgO below ~1500 K and formation of modified Ludwigite (mLd)-type $Mg_2Cr_2O_5$ + Cr_2O_3 above ~1500 K. Above 20 GPa, only a single phase with $CaTi_2O_4$-type structure of $MgCr_2O_4$ was observed at 1400-2000 K. A second-order Birch-Murnaghan fit to the pressure-volume data for the $CaTi_2O_4$-type phase of $MgCr_2O_4$ yields zero-pressure volume (V_0) = 264.4(8) Å^3 and bulk modulus (K_0) = 185.4(4) GPa, and for the $CaTi_2O_4$-type structure of natural $(Mg,Fe)(Al,Cr)_2O_4$ yields V_0 = 261(1) Å^3 and K_0 = 175.4(2) GPa. A second-order Birch-Murnaghan fit to the pressure-volume data for mLd-type $Mg_2Cr_2O_5$ yields V_0 = 338.9(8) Å^3 and K_0 = 186.5(6) GPa. Our high-pressure phase study of the

chromite spinels can be used as an indicator for shock pressure in impact rocks and meteorites. The bulk modulus of the high pressure phases of $MgCr_2O_4$ and $FeCr_2O_4$ can help develop a thermodynamic model for Mg and Fe endmember spinels in the upper mantle and transition zone.

Keywords

Magnesiochromite, chromite, $CaTi_2O_4$ phase, modified Ludwigite phase, equation of state.

Introduction

Chromite spinels $(Mg,Fe)Cr_2O_4$ are found in peridotite from the Earth's mantle. They also occur in layered ultramafic intrusive rocks (Gu and Wills 1988) and in metamorphic rocks such as serpentinites (Pearre and Heyl 1960). Chromite is commonly associated with olivine, magnetite, and corundum (Guilbert et al. 1986). Although typically present as accessory phases, chromite spinels are widely considered to be important petrogenetic indicators (Irvine 1965, 1967; Evans and Frost 1975; Sack and Ghiorso 1991; Bosi et al. 2008), and can point to certain regions in garnet lherzolite as targets for diamond exploration (Griffin and Ryan 1995, Stachel and Harris 2008). Yamamoto et al. (2008) found numerous exsolution lamellae of diopsidic clinopyroxene and coesite in podiform chromitites from the Luobusa ophiolite. To produce such exsolution features, it is necessary to incorporate SiO_2 and CaO components in the host chromite or its precursor. In fact, natural chromites contain only 0.6 wt.% SiO_2 and the CaO content is less than several tens of ppm (Arai and Yurimoto 1994). However, $MgCr_2O_4$-rich $CaTi_2O_4$-type (CT)/ $CaFe_2O_4$-type (CF) phase can contain Ca, Si, Ti, and Fe as $CaFe_2O_4$ and $CaTi_2O_4$ solid solutions (Chen et al. 2003a, 2003b). Those exsolution lamellae were explained by the association of high pressure minerals (diamond, clinopyroxene and coesite) with chromites in the podiform chromitites of the Luobusa

ophiolite by the inverse transformation from CT/CF phase to chromite by a mantle upwelling process (Yang et al. 2007; Yamamoto et al. 2009; Arai, 2010, 2013; Satukawa et al. 2015; Zhang et al. 2017). It has been suggested that high pressure and high temperature phases of chromite spinel are likely present in the deep mantle (Yamamoto et al. 2008; Satukawa et al. 2015; Zhang et al. 2017). This makes it geologically important to determine the equation of state (EOS) of these high pressure and high temperature phases of chromite spinel. Furthermore, studying the equations of state of high pressure phases of chromite is essential for understanding the bulk modulus and potentially for thermodynamic models of deep Earth and planetary materials. It is known that natural chromites exhibit solid solution in the $FeCr_2O_4$-$MgCr_2O_4$ system. Synthetic chromites, on the other hand, can readily be prepared as pure end-member phases such as $MgCr_2O_4$, eliminating the compositional variation in the final products.

Chromite spinel with the general formula ACr_2O_4 (where A is divalent metal) has a normal spinel structure with a tetrahedral coordination of the divalent metal ions and an octahedral coordination of chromium ions (Romeijn 1953; Miyahara and Ohnishi 1956; Sawaoka et al. 1971). The divalent metal ions can be Fe, Mg, Zn or Mn. Natural chromite is also a common mineral in many meteorites (Rubin 1997). More importantly, it has high degree of resistance against weathering and diagenesis, and is the only mineral surviving in a meteorite embedded within Middle Ordovician limestones (Thorslund et al. 1984). In a recent study of the shock veins of the Suizhou meteorite, Chen et al. (2003a, 2003b) reported that chromite spinel transforms to the CF-type structure at 12.5 GPa and to the CT-type structure above 20 GPa.

Due to their importance in the geosciences, physics, materials science, and crystallography, properties of chromite spinels have been studied extensively both theoretically and experimentally.

Ab initio calculation has been performed to examine the phase transformation of chromite (Catti et al. 1999). The simulation showed that chromite can dissociate to constituent oxides at high pressures and room temperature. Wang et al. (2002) first studied the magnesiochromite ($MgCr_2O_4$) spinel at high pressure using Raman and reported that this spinel underwent a phase transformation to CF or CT structure at 14.2 GPa. The complete transition took place at 30.1 GPa. However, the transformation of $MgCr_2O_4$ to CF or CT phase at room temperature was not supported by a recent in situ experimental study (Yong et al. 2012). Instead, a polymorphic phase transition from cubic to tetragonal structure was reported for $MgCr_2O_4$ at 23.5 GPa and room temperature (Yong et al. 2012) and at a much lower pressure (12 GPa) for chromite ($FeCr_2O_4$) (Kyono et al. 2012). A recent study on chromite ($FeCr_2O_4$) showed that chromite dissociates to modified Ludwigite-type $Fe_2Cr_2O_5$ phase + corundum-type Cr_2O_3 at 12-16 GPa. The assemblage is then transformed at 17-18 GPa to CF (space group *Pnma*)-type structure below 1573 K, or to CT (space group *Cmcm*)-type structure above 1573 K (Ishii et al. 2014). Another recent study on magnesiochromite ($MgCr_2O_4$) showed different phase behaviors (Ishii et al. 2015). $MgCr_2O_4$ dissociates into a mixture of new modified Ludwigite (mLd)-type $Mg_2Cr_2O_5$ phase (space group *Pbam*) + corundum-type Cr_2O_3 at 1273–1873 K, but, at temperature < l273 K, it decomposes into MgO periclase + corundum-type Cr_2O_3 at 12-15 GPa. At about 17–19 GPa, the mixture of mLd-type $Mg_2Cr_2O_5$ phase + corundum-type Cr_2O_3 transforms to a CT-type single phase. Note that the CF-type structure of $MgCr_2O_4$ was not observed in that study (Ishii et al. 2015).

Therefore, in this study we report and compare phase diagram of $MgCr_2O_4$ and the equations of state of $CaTi_2O_4$-type structure of $MgCr_2O_4$ and of natural $(Mg,Fe)(Al,Cr)_2O_4$, and mLd-type $Mg_2Cr_2O_5$ phase at mantle pressures.

This is the peer-reviewed, final accepted version for American Mineralogist, published by the Mineralogical Society of America.
The published version is subject to change. Cite as Authors (Year) Title. American Mineralogist, in press.
DOI: https://doi.org/10.2138/am-2021-7853. http://www.minsocam.org/

Experiments

Synthetic magnesiochromite ($MgCr_2O_4$) and natural chromite $(Mg,Fe)(Al,Cr)_2O_4$ were used as starting materials. The $MgCr_2O_4$ was obtained from the same batch used in our previous study (Yong et al. 2012). Natural chromite $(Mg,Fe)(Al,Cr)_2O_4$ (Sudbury, Ontario) with a chemical formula of $Mg_{0.52(2)}Fe_{0.61(2)}Mn_{0.01(0)}Ti_{0.01(0)}Al_{0.58(1)}Cr_{1.30(1)}O_4$ was determined by electron microprobe at University of Western Ontario. The chromite sample was first ground to mm-sized grains and then dried in an oven at 473 K for at least 12 h. In order to separate the chromite from other accessory minerals, pure chromite grains were hand-picked with a needle under a microscope.

The mm-sized samples were ground to 1-3 μm fine powder and mixed with ~10 wt% gold for use as a pressure calibrant. The pressure was determined by the equation of state of gold (Fei et al. 2007). Mixtures of the samples and gold were then loaded into a ~120 μm hole drilled in a rhenium gasket. Neon was also loaded as a pressure medium in the diamond-anvil cell (DAC) using the GSECARS high-pressure gas loading system (Rivers et al. 2008). In situ high-pressure and high-temperature X-ray diffraction (XRD) experiments were performed at 13-ID-D, GSECARS, Advanced Photon Source (APS) of Argonne National Laboratory (Prakapenka et al. 2008). A double-sided laser heating method was employed with synchrotron XRD. The temperature of the sample heated with focused spot in a diameter of about 20 μm was measured from both sides by spectroradiometry. The samples were probed with a monochromatic X-ray beam with a wavelength of 0.3344 Å and a 3×2 μm cross-section. The X-ray beam was ensured to be in the center of the heating spot by carefully aligning optical paths using X-ray induced fluorescence on the sample. A Mar-165 CCD detector was used to collect the XRD images. The sample-to-detector distance and orientation of the detector were calibrated using CeO_2 and LaB_6 powder. The

DIOPTAS software was used for calibration and integration of the diffraction images (Prescher and Prakapenka 2015).

Results and Discussion

In the high pressure and high temperature experiments conducted on synthetic $MgCr_2O_4$, we observed dissociation of $MgCr_2O_4$ to Cr_2O_3 + MgO at ~15 GPa and temperature below 1440 K, whereas mLd-type $Mg_2Cr_2O_5$ + Cr_2O_3 was observed when the sample was heated above 1600 K. At pressure above 20 GPa, only a single phase, $CaTi_2O_4$-type (CT) structure was observed at the temperature of 1400-2000 K (Fig. 1). The tetragonal phase of $MgCr_2O_4$ was also observed above 23.5 GPa and ambient temperature (Fig. 1). Our synthesis result is in broad agreement with previously reported high pressure and high temperature experiments and the obtained phase diagram is shown in Fig. 2 (Kyono et al. 2012, Yong et al. 2012, Ishii et al. 2015). The discrepancy of phase boundary between MgO+Cr_2O_3 and mLd-type $Mg_2Cr_2O_5$ + Cr_2O_3 could be resulted from different temperature determination method. In order to determine the EOS of the polymorphs of $MgCr_2O_4$, the syntheses were performed within the stability field of the desired polymorph. The CT phase of $MgCr_2O_4$ was synthesized at ~45 GPa and ~1800 K, natural $(Mg,Fe)(Al,Cr)_2O_4$ was compressed to ~40 GPa and heated at ~1800 K, and mLd-type $Mg_2Cr_2O_5$ structure was produced at ~16 GPa and ~1500 K, respectively. The phases synthesized at high pressure and high temperature were then decompressed to ambient conditions over a period of ~6-8 hours and a dense set of XRD patterns was collected during decompression.

The cubic spinel phase of $MgCr_2O_4$ transformed completely to an orthorhombic CT structure at ~45 GPa and ~1800 K under hydrostatic conditions. The observed and calculated peak positions of CT structure of $MgCr_2O_4$ retained at ambient conditions are shown in Table 1. The unit-cell

lattice parameters of the CT structure of $MgCr_2O_4$ at ambient conditions are a_0 = 2.86464(8) Å, b_0 = 9.51504(5) Å, and c_0 = 9.6981(6) Å. The obtained unit-cell lattice parameters at ambient conditions are close to those determined by Ishii et al. (2015) (a_0 = 2.85107(2) Å, b_0 = 9.48930(8) Å and c_0 = 9.67853(8) Å), which confirms the synthesis of CT phase. The unit-cell lattice parameters and the volumes of synthesized CT phase of $MgCr_2O_4$ at different pressures are tabulated in Table S1.

Similarly, natural $(Mg,Fe)(Al,Cr)_2O_4$ transformed completely to CT-type structure (*Cmcm*) at ~40 GPa and ~1800 K. The unit-cell lattice parameters for the CT phase of natural $(Mg,Fe)(Al,Cr)_2O_4$ at ambient conditions are a_0 = 2.8575(6) Å, b_0 = 9.4506(6) Å, and c_0 = 9.6641(7) Å, which are slightly lower than those of the CT phase of $MgCr_2O_4$ (see above) and CT phase of $FeCr_2O_4$ (a_0 = 2.8845(1) Å, b_0 = 9.5207(2) Å, and c_0 = 9.7532(2) Å) (Ishii et al. 2014). The unit-cell lattice parameters and the volumes of the CT phase of natural $(Mg,Fe)(Al,Cr)_2O_4$ at different pressures are listed in Table S2.

To evaluate the pressure derivative of the bulk modulus (K_0') of CT-type phases of both the compounds we plotted the normalized pressure versus Eulerian strain. Our results show a horizontal relationship for both compounds, suggesting a value of 4 for the pressure derivative of the isothermal bulk modulus (Fig. 3). This allows us to fit the pressure-volume data with a second-order Birch-Murnaghan EOS and the results are shown in Fig. 3 and Table 2. Comparing the EOS fitting curves of the CT phase of $MgCr_2O_4$, natural chromite $(Mg,Fe)(Al,Cr)_2O_4$ and $FeCr_2O_4$ (Ishii et al. 2014) indicate that natural chomite $(Mg,Fe)(Al,Cr)_2O_4$ has the lowest volume whereas $FeCr_2O_4$ has the highest volume (Fig. 3). In the CT phase the coordination number of Cr is suggested to be 6 (i.e. it occupies octahedral sites) whereas the coordination number of Mg and Fe

This is the peer-reviewed, final accepted version for American Mineralogist, published by the Mineralogical Society of America.
The published version is subject to change. Cite as Authors (Year) Title. American Mineralogist, in press.
DOI: https://doi.org/10.2138/am-2021-7853. http://www.minsocam.org/

is 6+2 (they occupy bicapped trigonal prism sites) based on the results of Ishii et al. (2014). Furthermore, our high-temperature data of CT phase of Mg_2CrO_4 fitted to the second-order EOS yield V_0 = 266.5(2) Å^3 at 1200 K, V_0 = 268.4(2) Å^3 at 1400 K, and V_0 = 270.2(2) Å^3 at 1550 K (Fig. 4). High-temperature data of CT phase of natural $(Mg,Fe)(Al,Cr)_2O_4$ fitted to the second-order EOS yield V_0 = 262.8(1) Å^3 at 1600 K (Fig. 4).

From our experiments, the mLd-type $Mg_2Cr_2O_5$ + Cr_2O_3 phase that we synthesized at high pressure and high temperature conditions is mixed with original chromite spinel phase and sometimes with $CaTi_2O_4$-type phase. The persistence of original spinel structure was attributed to slow kinetics and short heating duration (the duration of each heating cycle was around 1 hour). On the other hand, growth of minor amounts of $CaTi_2O_4$-type structure may be attributed to brief temperature fluctuations during the synthesis process. However, the limited amounts of CT phase at this pressure and temperature range did not affect the data processing. The mLd-type $Mg_2Cr_2O_5$ is stable in a narrow P-T range (Fig. 2) and, therefore, it is difficult to obtain a pure phase of mLd-type $Mg_2Cr_2O_5$. For our purposes, the data quality of the mixed phase is sufficient to determine the EOS. Observed and calculated peak positions of mLd-type $Mg_2Cr_2O_5$, Cr_2O_3 and CT-type structure of $MgCr_2O_4$ at ambient conditions is shown in Table S3.

In addition, $MgCr_2O_4$ dissociates into MgO + Cr_2O_3 at similar pressures but lower temperatures than those at which mLd-type $Mg_2Cr_2O_5$ + Cr_2O_3 form (Fig. 2). With the large number of pressure-volume data collected for Cr_2O_3, we were also able to determine the EOS of Cr_2O_3 phase and compare with the EOS determined by Dera et al. (2011). Fig. 5 shows the isothermal compression curve of Cr_2O_3 phase from the same XRD patterns that are used to determine the EOS of mLd-type $Mg_2Cr_2O_5$ phase. The Birch-Murnaghan EOS fitting of our Cr_2O_3 phase is in very good

agreement with previously reported EOS of Cr_2O_3 (Dera et al. 2011). This confirms that our data collected from a mixture of phases are of high quality.

The variation of volume with pressure for mLd-type $Mg_2Cr_2O_5$ phase is tabulated in Table S4, and the EOS is presented in Fig. 6. The plot of normalized pressure versus Eulerian strain indicates that the value of K_0' is 4 as the data points have a linear distribution with a derivative equal to zero. Pressure-volume data fitted to a second order Birch-Murnaghan EOS yield $V_0 = 338.9(8)$ Å^3 and $K_0 = 186.5(6)$ GPa at room temperature. Our limited high temperature data fitted to the same second order Birch-Murnaghan EOS yield $V_0 = 348.5(8)$ Å^3.

The rates of change in unit-cell lattice parameters for two CT and one mLd phases are slightly different from each other (Fig. 7), suggesting that axial compression of the orthorhombic phases of these compounds is anisotropic. The CT structure has similar compressibility in *a*- and *b*-axis but different in *c*-axis, whereas mLd-type $Mg_2Cr_2O_5$ phase has same compressibility in *a*- and *c*-axis but different in *b*-axis.

The density profiles of $FeCr_2O_4$, $MgCr_2O_4$, $(Mg,Fe)(Al,Cr)_2O_4$ and their high pressure phases including mLd and CT phases calculated at room temperature and high tempeatures are plotted in Fig. 8. Low and high pressure $FeCr_2O_4$ phases show significantly higher densities than $MgCr_2O_4$ phases (Fig. 8). The CT phase of $MgCr_2O_4$ has higher density than the mLd-type $Mg_2Cr_2O_5$ phase. This is reasonable as the mLd phase is the lower pressure phase of $MgCr_2O_4$ and may be found at shallower depth in Earth's mantle compared to the CT phase of $MgCr_2O_4$. A similar trend is also observed for $FeCr_2O_4$ phases. It is interesting to note that the CT phase of $(Mg,Fe)(Al,Cr)_2O_4$ is denser than the CT phase of $MgCr_2O_4$, but still less dense than the CT phase of $FeCr_2O_4$. This

relationship can be attributed to the substitution of Al from Fe in the CT phase of $(Mg,Fe)(Al,Cr)_2O_4$ compared to the Fe-free CT phase of $MgCr_2O_4$, and the Fe-rich CT phase of $FeCr_2O_4$. Furthermore, the presence of Al makes the high-pressure phase of chromium spinel more compressible. As a result, the density of CT phase of $(Mg,Fe)(Al,Cr)_2O_4$ with the presence of Al is close to that of chromite ($FeCr_2O_4$). Therefore, the appearance of appreciable amounts of the $(Mg,Fe)(Al,Cr)_2O_4$ polymorphs inside the planetary interiors should have an observable effect on physical properties due to their high density contrast. Furthermore, the high-temperature data of CT phase of $MgCr_2O_4$ and $(Mg,Fe)(Al,Cr)_2O_4$ and the mLd-type $Mg_2Cr_2O_5$ phase show about 2-3.0% density drop, compared to their room-temperature data.

To evaluate the effects of bulk sound velocity of $FeCr_2O_4$, $MgCr_2O_4$, $(Mg,Fe)(Al,Cr)_2O_4$ and their high pressure phases at high pressures, we used the obtained densities and derived EOS of those phases at room and high temperatures to calculate their bulk sound velocities and the results are shown in Fig. 9. The bulk sound velocities of $MgCr_2O_4$ spinel show highest values whereas CT phase of $FeCr_2O_4$ and $(Mg,Fe)(Al,Cr)_2O_4$ are among the lowest ones. In addition, transformation of $MgCr_2O_4$ to mLd-type $Mg_2Cr_2O_5$ phase at ~15 GPa and to CT phase of $MgCr_2O_4$ at ~20 GPa would drop the velocity significantly. Note that the mLd phase of $Mg_2Cr_2O_5$ has comparable bulk sound velocity as $FeCr_2O_4$ spinel at room temperature and at upper mantle pressures. Transformation to CT phase of $FeCr_2O_4$, $MgCr_2O_4$, and $(Mg,Fe)(Al,Cr)_2O_4$ all result in much lower bulk sound velocities. Importantly, high-temperature bulk sound velocity of mLd phase of $Mg_2Cr_2O_5$ and CT phase of $MgCr_2O_4$ and $(Mg,Fe)(Al,Cr)_2O_4$ show higher values than their room-temperature ones, suggesting that high temperature (1550-1700 K) enhances the bulk sound velocity about 0.7-1.4%. In summary, our study suggests distinct density variations on $FeCr_2O_4$,

$MgCr_2O_4$, and $(Mg,Fe)(Al,Cr)_2O_4$ polymorphs without significant differences in their bulk sound velocities.

Implications

High-pressure phases of chromite phases (CF and CT) were found in Suizhou meteorite (Chen et al. 2003a, 2003b) and Luobusa ophiolite (Satukawa et al. 2015; Zhang et al. 2017). Our high-pressure synthesis study show that the chromite spinels transform to modified Ludwigite (mLd)-type phase + Cr_2O_3 at~15 GPa and then to $CaTi_2O_4$-type phase above 20 GPa, in good agreement with previous reports (Ishii et al. 2014, 2015). The experimentally calibrated high-pressure phase transformations of $FeCr_2O_4$, $MgCr_2O_4$, and $(Mg,Fe)(Al,Cr)_2O_4$ series minerals provide a pressure gauge for shock-metamorphosed rocks and meteorites and also for mantle-derivative rocks. Previous EOS studies on spinels showed compositional dependence on the bulk moduli of Fe and Mg end-member of spinels and post-spinel phases (Siersch et al. 2017). In this study, it is extended beyond the post-spinel phases and even compared to the aluminum-bearing chromite spinel. The Fe-rich CT phase is indeed less compressible than Mg-rich and Al-bearing CT phases. The substitution of Mg and Al for Fe in the CT phase not only influences the bulk modulus but also the volumes. It is therefore an important implication for modeling the thermodynamic properties of high-pressure chromium spinel phases at high pressure and temperature conditions. In addition, determination of the isothermal bulk modulus is critical for obtaining the other thermodynamic parameters such as vibrational Grüneisen parameter. Eventually, the newly determined bulk moduli for two high pressure phases of $MgCr_2O_4$, and one high pressure phase of $(Mg,Fe)(Al,Cr)_2O_4$ in this study will help to facilitate the determination of the physical properties of the high pressure forms of chromite spinels obtained from deep mantle such as the Tibetan ophiolites (Zhang et al. 2017) and/or meteorites (Chen et al. 2003a, b).

Acknowledgements

We thank the constructive comments from Tony Withers, the two anonymous reviewers and the editor that help improve the quality of this manuscript. This work was supported by NSERC and performed at GeoSoilEnviroCARS (Sector 13), Advanced Photon Source (APS), Argonne National Laboratory. GeoSoilEnviroCARS is supported by the National Science Foundation - Earth Sciences (EAR-1128799) and Department of Energy- GeoSciences (DE-FG02-94ER14466). This research used resources of the Advanced Photon Source, a U.S. Department of Energy (DOE) Office of Science User Facility operated for the DOE Office of Science by Argonne National Laboratory under Contract No. DE-AC02-06CH11357. Use of the COMPRES-GSECARS gas loading system was supported by COMPRES under NSF Cooperative Agreement EAR 11-57758 and by GSECARS through NSF grant EAR-1128799 and DOE grant DE-FG02-94ER14466. This research used resources of the Advanced Photon Source, a U.S. Department of Energy (DOE) Office of Science User Facility operated for the DOE Office of Science by Argonne National Laboratory under Contract No. DE-AC02-06CH11357.

References

Angel, R.J. (2000) Equations of state. In R.M. Hazen and R.T. Downs (eds.), High-pressure and high-temperature crystal chemistry. Reviews in Mineralogy and Geochemistry, 41:35-60.

Arai, S. (2010) Chromitites : An Enigmatic Mantle Rock Type. J. Geography. 119 (2), 392-410.

Arai, S. (2013) Conversion of low-pressure chromitites to ultrahigh-pressure chromitites by deep recycling: A good inference. Earth and Planetary Science Letters, 379, 81-87.

Bosi, F., Hålenius, U., and Skogby, H. (2008) Stoichiometry of synthetic ulvöspinel single crystals. American Mineralogist, 93, 1312–1316.

Catti, M., Freyria, F., Zicovich, C., and Dovesi, R. (1999) High-pressure decomposition of MCr_2O_4 spinels (M = Mg, Mn, Zn) by ab initio methods. Physics and Chemistry of minierals, 26, 389-395.

Chen, M., Shu, J., Mao, H.K., Xie, X., and Hemley, R.J. (2003a) Natural Occurrence and Synthesis of Two New Postspinel Polymorphs of Chromite. Proceedings of the National Academy of Sciences, 100 (25), 14651-14654.

Chen, M., Shu, J., Xie, X., Mao, H. (2003b) Natural $CaTi_2O_4$-structured $FeCr_2O_4$ polymorph in the Suizhou meteorite and its significance in mantle mineralogy. Geochimica et Cosmochimica Acta, 67, 3937-3942.

Dera, B. Lavina, Y. Meng, P. V. B, J. (2011) Structural and electronic evolution of Cr_2O_3 on compression to 55GPa. Solid State Chemistry. 184, 3040-3055.

Evans, B.W., and Frost, B.R. (1975) Chrome spinels in progressive metamorphism-a preliminary analysis. Geochimica et Cosmochimica Acta, 39, 959-972.

Fei, Y., Ricolleau, A., Frank, M., Mibe K., Shen, G. and Prakapenka, V. (2007), Toward an internally consistent pressure scale, Proc. Natl. Acad. Sci.U.S.A.,104, 9182–9186.

Guilbert, John M., and Park, Charles F., Jr. (1986) The Geology of Ore Deposits, p. 210-217. Freeman, New York.

Griffin, W.L., and Ryan, C.G. (1995) Trace Elements in Indicator Minerals: Area Selection and Target Evaluation in Diamond Exploration. Journal of Geochemical Exploration, 53, 311-337.

Gu, F. and Wills, B. (1988) Chromite- mineralogy and processing. Minerals Engineering, 1(3), 235-240.

Irvine, T. (1965) Chromian spinel as a petrogenetic indicator: part 1. Theory. Canadian Journal of Earth Sciences, 2, 648–672.

Irvine, T. (1967) Chromian spinel as a petrogenetic indicator: Part 2 Petrologic applications. Canadian Journal of Earth Sciences, 4, 71–103.

Ishii, T., Kojitani, H., Tsukamoto, S., Fujino, K., Mori, D., Inaguma, Y., Tsujino, N., Yoshino, T., Yamazaki, D., Higo, Y., Funakoshi, K., Akaogi, M. (2014) High-pressure phase transitions in $FeCr_2O_4$ and structure analysis of new post-spinel $FeCr_2O_4$ and $Fe_2Cr_2O_5$ phases with meteoritical and petrological implications. American Mineralogist, 99 (8-9), 1788–1797.

Ishii, T., Kojitani, H., Fujino, K., Yusa, H., Mori, D., Inaguma, Y., Matsushita, Y., Yamaura, K., Akaogi, M. (2015) High-pressure high-temperature transitions in $MgCr_2O_4$ and crystal structures of new $Mg_2Cr_2O_5$ and post-spinel $MgCr_2O_4$ phases with implications for ultrahigh-pressure chromitites in ophiolites. American Mineralogist, 100(1), 59-65.

Kyono, A., Gramsch, S., Yamanaka, T., Ikuta, D., Ahart, M., Mysen, B., Mao, H.K., Hemley, R. (2012) The influence of the Jahn–Teller effect at Fe^{2+} on the structure of chromite at high pressure. Physics and Chemistry of Minerals, 39, 131–141.

Miyahara, S., and Ohnishi, H. (1956) Cation arrangement and magnetic properties of copper ferrite-chromite series. Journal of the Physical Society of Japan, 11, 1296-1302.

Pearre, N.C., and Heyl, A.V., Jr. (1960) Chromite and other mineral deposits in serpentine rocks of the Piedmont Upland, Maryland, Pennsylvania, and Delaware. U.S. Geological Survey Bulletin 1082-K, 707-833.

Prakapenka V. B., Kubo A., Kuznetsov A., Laskin A., Shkurikhin O., Dera P., Rivers M. L. and Sutton S. R. (2008) Advanced flat top laser heating system for high pressure research at

GSECARS: Application to the melting behavior of germanium. High Pressure Research, 28, 225-235.

Prescher, C. and Prakapenka, V. B. (2015) DIOPTAS: a program for reduction of two-dimensional X-ray diffraction data and data exploration. High Pressure Research, 35 (3), 223-230.

Rivers, R., Prakapenka, V. B., Kubo, A., Pullins, C., Holl, C. M., Jacobsen, S. D. (2008) The COMPRES/GSECARS gas-loading system for diamond anvil cells at the Advanced Photon Source. High Pressure Research, 28 (3), 273-292.

Romeijn, F.C. (1953) Physical and crystallographical properties of some spinels. Philips Reserve Report, 8, 304-342.

Rubin A. E. (1997) Mineralogy of meteorite groups. Meteoritics & Planetary Science, 32, 231–247.

Sack, R.O., and Ghiorso, M.S. (1991) Chromian spinels as petrogenetic indicators: thermodynamics and petrological applications. American Mineralogist, 76, 827-847.

Satsukawa, T., Griffin, W.L., Piazolo, S., O'Reilly, S.Y. (2015) Messengers from the deep: fossil wadsleyite–chromite microstructures from the Mantle Transition Zone. Sci. Rep.5, 16484.

Sawaoka, A., Saito, S., Inoue, K., and Asada, T. (1971) Effect of High Pressure on the Lattice Constants of Chromites Having The Spinel Structure. Material Review Bulletin, 6 (2), 97-102.

Shieh, S.R., Dorfman, S.M., Kubo, A., Prakapenka, V.B., Duffy, T.S. (2011) Synthesis and equation of state of post-perovskites in the $(Mg,Fe)_3Al_2Si_3O_{12}$ system. Earth and Planetary Science Letters, 312, 422–428.

Siersch, N.C., Ballaran, T.B., Uenver-Thiele, L., Woodland, A.B. (2017) Compressibility and high-pressure structural behavior of $Mg_2Fe_2O_5$. American Mineralogist, 102, 845-850.

Stachel, T., and Harris, J.W. (2008) The origin of cratonic diamonds – constraints from mineral inclusions. Ore Geology Reviews, 34, 5–32.

Thorslund P., Wickman, F.E., Nyström, J.O. (1984) The Ordovician chondrite from Brunflo, central Sweden, I. General description and primary minerals. Lithos, 17, 87–100.

Wang, Z., O'Neill, H., Lazor, P., Saxena, S.K. (2002) High pressure Raman spectroscopic study of spinel $MgCr_2O_4$. Journal of Physics and Chemistry of Solids, 63, 2057–2061.

Yamamoto, S., Komiya, T., Hirose, K., Maruyama, S. (2008) Coesite and clinopyroxene exsolution lamellae in chromites: In-situ ultrahigh-pressure evidence from podiform chromitites in the Luobusa ophiolite, southern Tibet. Lithos, 109, 314–322.

Yang, J.S., Dobrzhinetskaya, L., Bai, W.-J., Fang, Q.-S., Robinson, P.T., Zhang, J., Green, H.W. (2007) Diamond- and coesite-bearing chromitites from the Luobusa ophiolite. Tibet. Geo., 35, 875–878.

Yong, W., Botis, S., Shieh, S. R., Shi, W., Withers, A. C. (2012) Pressure-induced phase transition study of magnesiochromite (MgCr2O4) by Raman spectroscopy and X-ray diffraction. Physics of the Earth and Planetary Interiors, 196, 75-82.

Zhang, Y., Jin, Z., Griffin, W.L., Wang, C., Wu, Y. (2017) High-pressure experiments provide insights into the Mantle Transition Zone history of chromitite in Tibetan ophiolites, Earth and Planetary Science Letters 463, 151–158.

List of figure captions

Figure 1: X-ray diffraction patterns of high pressure phases synthesized at various pressure and temperature conditions from $MgCr_2O_4$ as a starting material. The synthesized phases are: (I) $MgCr_2O_4$ (II) Tetragonal $MgCr_2O_4$ (III) Cr_2O_3+MgO (IV) Cr_2O_3+$Mg_2Cr_2O_5$ (V) $CaTi_2O_4$-type structure of $MgCr_2O_4$. Chr denotes $MgCr_2O_4$, mLd denotes $Mg_2Cr_2O_5$, Cr denotes Cr_2O_3, Au denotes gold, Ne denotes neon, CT denotes $CaTi_2O_4$-type phase and TT denotes tetragonal $MgCr_2O_4$. Vertical bars are the calculated peak positions for the different phases present.

Figure 2: Phase diagram of $MgCr_2O_4$. The solid lines are phase boundaries from this study.

The red dotted lines are from Ishii et al. (2015).

Figure 3: Volumes as a function of pressure for the CT phase of $MgCr_2O_4$, natural $(Mg,Fe)(Al,Cr)_2O_4$ and synthetic $FeCr_2O_4$. (i) Natural $(Mg,Fe)(Al,Cr)_2O_4$: ambient volume V_0 = 261(1) Å^3, Bulk Modulus K_0 = 175.4(2) GPa, and K_0' = 4; (ii) $MgCr_2O_4$: V_0 = 264.4(8) Å^3, K_0 = 185.4(4) GPa, and K_0' = 4; and (iii) synthetic $FeCr_2O_4$ (Ishii et al. 2014) : V_0 = 266.95 Å^3, K_0 = 199 GPa, and K_0' = 4. Pressure derivative of the isothermal bulk modulus (K_0') was determined using normalized pressure and Eulerian Strain relationship for both CT phase of natural $(Mg,Fe)(Al,Cr)_2O_4$ (lower left inset a) and $MgCr_2O_4$ (upper right inset b).

Figure 4: Comparison between the Birch-Murnaghan EOS fit to volume of Cr_2O_3 as a function of pressure (this study) and that of Dera et al. (2011).

Figure 5: Pressure-volume relationship of modified Ludwigite-type $Mg_2Cr_2O_5$ phase. The inset shows linear relationship of normalized pressure and Eulerian strain for modified Ludwigite-type $Mg_2Cr_2O_5$ phase.

Figure 6: Compressibility of the (top) CT phase of $MgCr_2O_4$, (middle) CT phase of natural $(Mg,Fe)(Al,Cr)_2O_4$ and (bottom) modified Ludwigite-type $Mg_2Cr_2O_5$ at high pressures. The three phases all show weakly anisotropic behavior.

Figure 7: Density as a function of pressure for $MgCr_2O_4$, $FeCr_2O_4$, mLd-type $Mg_2Cr_2O_5$, CT phase of $MgCr_2O_4$, CT phase of $FeCr_2O_4$ and CT phase of natural $(Mg,Fe)(Al,Cr)_2O_4$. N chromite stands for natural $(Mg,Fe)(Al,Cr)_2O_4$.

Figure 8: Bulk sound velocity as a function of pressure for $MgCr_2O_4$, $FeCr_2O_4$, mLd-type $Mg_2Cr_2O_5$, CT phase of $MgCr_2O_4$, CT phase of $FeCr_2O_4$ and CT phase of natural $(Mg,Fe)(Al,Cr)_2O_4$. N chromite stands for natural $(Mg,Fe)(Al,Cr)_2O_4$.

Tables

Table 1: Calculated and observed *d*-spacings of synthesized CT phase of $MgCr_2O_4$ at ambient conditions.

$d_{obs.}$ (Å)	hkl	$d_{calc.}$ (Å)	Δd (Å)
4.8454 (2)	002	4.8491 (1)	-0.0037
4.2731 (1)	021	4.2713 (1)	0.0018
3.3979 (1)	022	3.3959 (1)	0.0019
2.7401 (3)	110	2.7431 (2)	-0.0029
2.6736 (1)	023	2.6738 (1)	-0.0002
2.6372 (1)	111	2.6394 (1)	-0.0021
2.3808 (2)	040	2.3788 (2)	0.0020
2.1631 (0)	024	2.1602 (2)	0.0028
2.1243 (1)	130	2.1259 (1)	-0.0016
2.0886 (2)	113	2.0913 (1)	-0.0027
2.0749 (2)	131	2.0765 (1)	-0.0020

1.9464 (2)	132	1.9469 (3)	-0.0005
1.8166 (1)	114	1.8164 (1)	0.0002
1.7971 (1)	025	1.7961 (1)	0.0009
1.7765 (3)	133	1.7761 (1)	0.0004
1.6169 (1)	006	1.6164 (3)	0.0005
1.5846 (1)	150	1.5851 (1)	-0.0006
1.5641 (2)	151	1.5643 (3)	-0.0002
1.5066 (4)	152	1.5066 (2)	-0.0005
1.5036 (1)	045	1.5032 (1)	0.0003
1.4321 (1)	135	1.4328 (1)	-0.0006
1.4243 (2)	063	1.4237 (1)	0.0006
1.3931 (2)	116	1.3925 (1)	0.0007
1.3775 (4)	202	1.3736 (1)	0.0039
1.3374 (2)	046	1.3369 (2)	0.0005
1.3262 (2)	154	1.3267 (1)	-0.0005
1.2832 (1)	136	1.2866 (1)	-0.0034
1.2612 (2)	223	1.2625 (1)	-0.0013
1.2269 (2)	240	1.2271 (1)	-0.0006
1.2164 (1)	241	1.2173 (1)	-0.0003
1.1955 (1)	047	1.1972 (2)	-0.0020
1.1901 (1)	080	1.1894 (2)	0.0007
1.1807 (4)	081	1.1805 (2)	0.0002
1.1611 (4)	137	1.1606 (1)	0.0004
1.1205 (1)	225	1.1197 (1)	0.0008

This is the peer-reviewed, final accepted version for American Mineralogist, published by the Mineralogical Society of America.
The published version is subject to change. Cite as Authors (Year) Title. American Mineralogist, in press.
DOI: https://doi.org/10.2138/am-2021-7853. http://www.minsocam.org/

1.1099 (1)	118	1.1087 (1)	0.0012

*Numbers in the parenthesis are the errors at the last digit.

Table 2: Comparison of volumes, bulk moduli and their pressure derivatives of CT phases, mLd-type $Mg_2Cr_2O_5$, and Cr_2O_3 obtained from this study and previous reports.

Polymorphs	V_0 (Å^3)	K_0 (GPa)	K_0'
CT phase of $MgCr_2O_4$	264.4(8)	185.4(4)	4.0
CT phase of natural $(Mg,Fe)(Al,Cr)_2O_4$	261.0(1)	175.4(2)	4.0
mLd-type $Mg_2Cr_2O_5$	338.9(8)	186.5(6)	4.0
CT phase of $FeCr_2O_4$ (Ishii et al. 2014)	285.22(1)	199.0(0)	4.0
Cr_2O_3	289.1(8)	214.0 (5)	4.7(2)
Cr_2O_3 (Dera et al. 2011)	288.6(2)	220.0 (4)	4.7(2)

This is the peer-reviewed, final accepted version for American Mineralogist, published by the Mineralogical Society of America.
The published version is subject to change. Cite as Authors (Year) Title. American Mineralogist, in press.
DOI: https://doi.org/10.2138/am-2021-7853. http://www.minsocam.org/

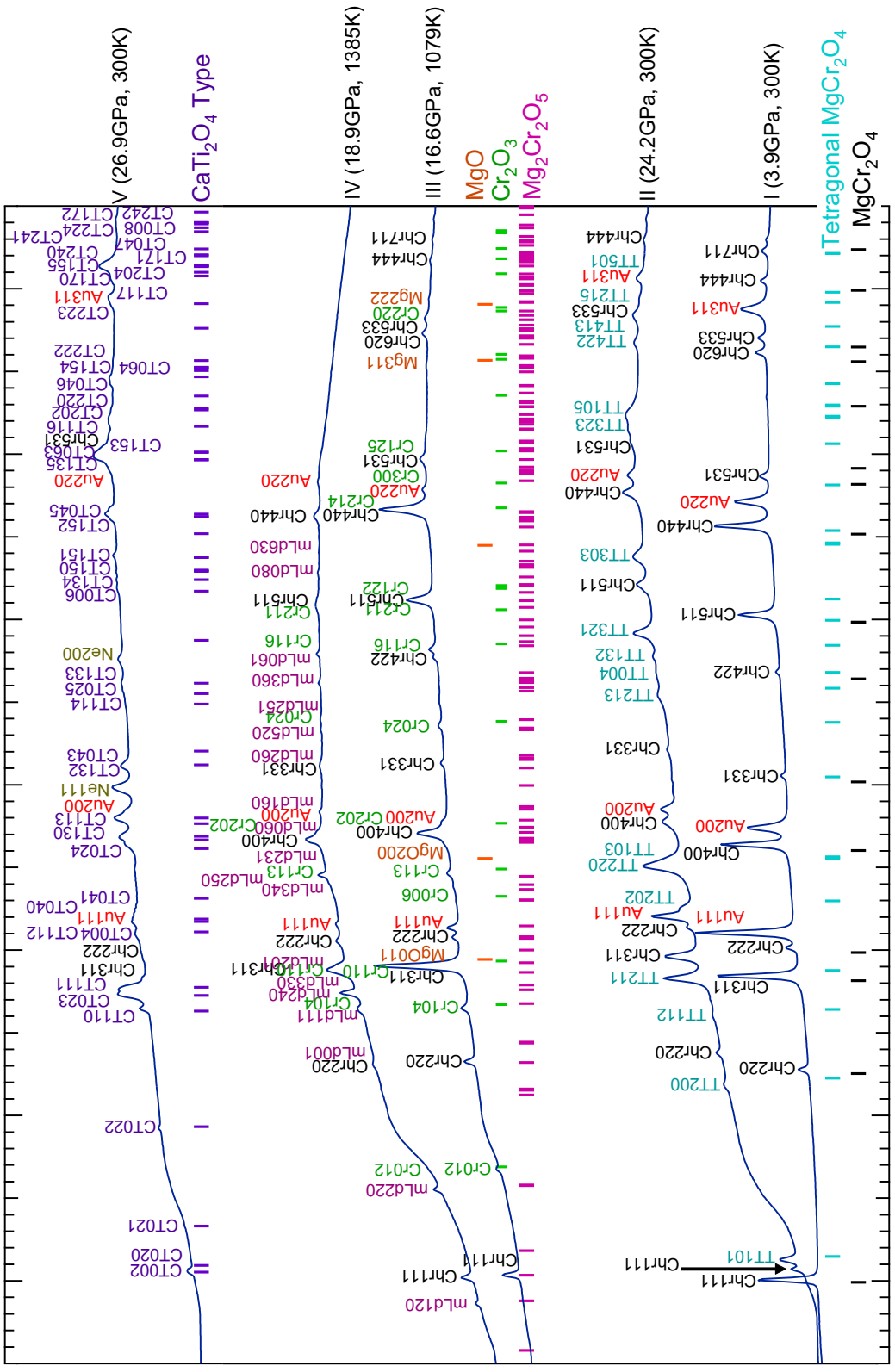

This is the peer-reviewed, final accepted version for American Mineralogist, published by the Mineralogical Society of America.
The published version is subject to change. Cite as Authors (Year) Title. American Mineralogist, in press.
DOI: https://doi.org/10.2138/am-2021-7853. http://www.minsocam.org/

Figure 1: X-ray diffraction patterns of high pressure phases synthesized at various pressure and temperature conditions from $MgCr_2O_4$ as a starting material. The synthesized phases are: (I) $MgCr_2O_4$ (II) Tetragonal $MgCr_2O_4$ (III) Cr_2O_3+MgO (IV) Cr_2O_3+$Mg_2Cr_2O_5$ (V) $CaTi_2O_4$-type structure of $MgCr_2O_4$. Chr denotes $MgCr_2O_4$, mLd denotes $Mg_2Cr_2O_5$, Cr denotes Cr_2O_3, Au denotes gold, Ne denotes neon, CT denotes $CaTi_2O_4$-type phase and TT denotes tetragonal $MgCr_2O_4$. Vertical bars are the calculated peak positions for the different phases present.

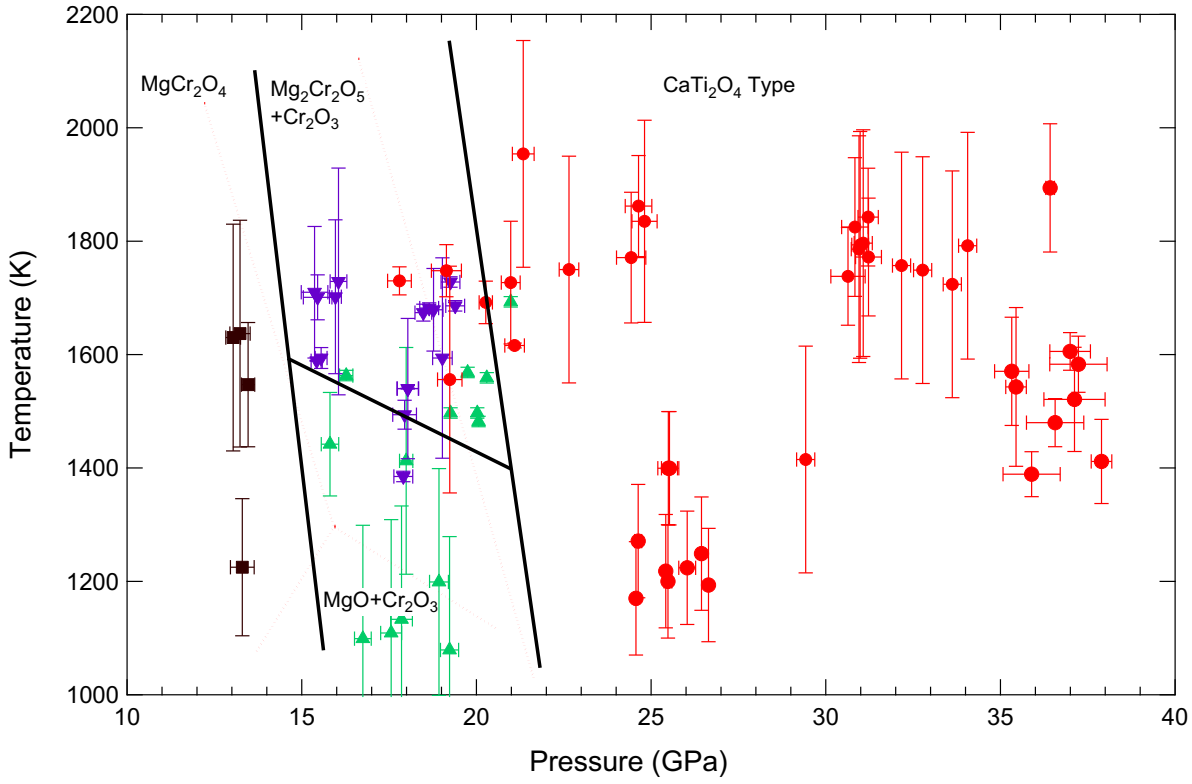

Figure 2: Phase diagram of $MgCr_2O_4$. The solid lines are phase boundaries from this study. The red dotted lines are from Ishii et al. (2015).

This is the peer-reviewed, final accepted version for American Mineralogist, published by the Mineralogical Society of America.
The published version is subject to change. Cite as Authors (Year) Title. American Mineralogist, in press.
DOI: https://doi.org/10.2138/am-2021-7853. http://www.minsocam.org/

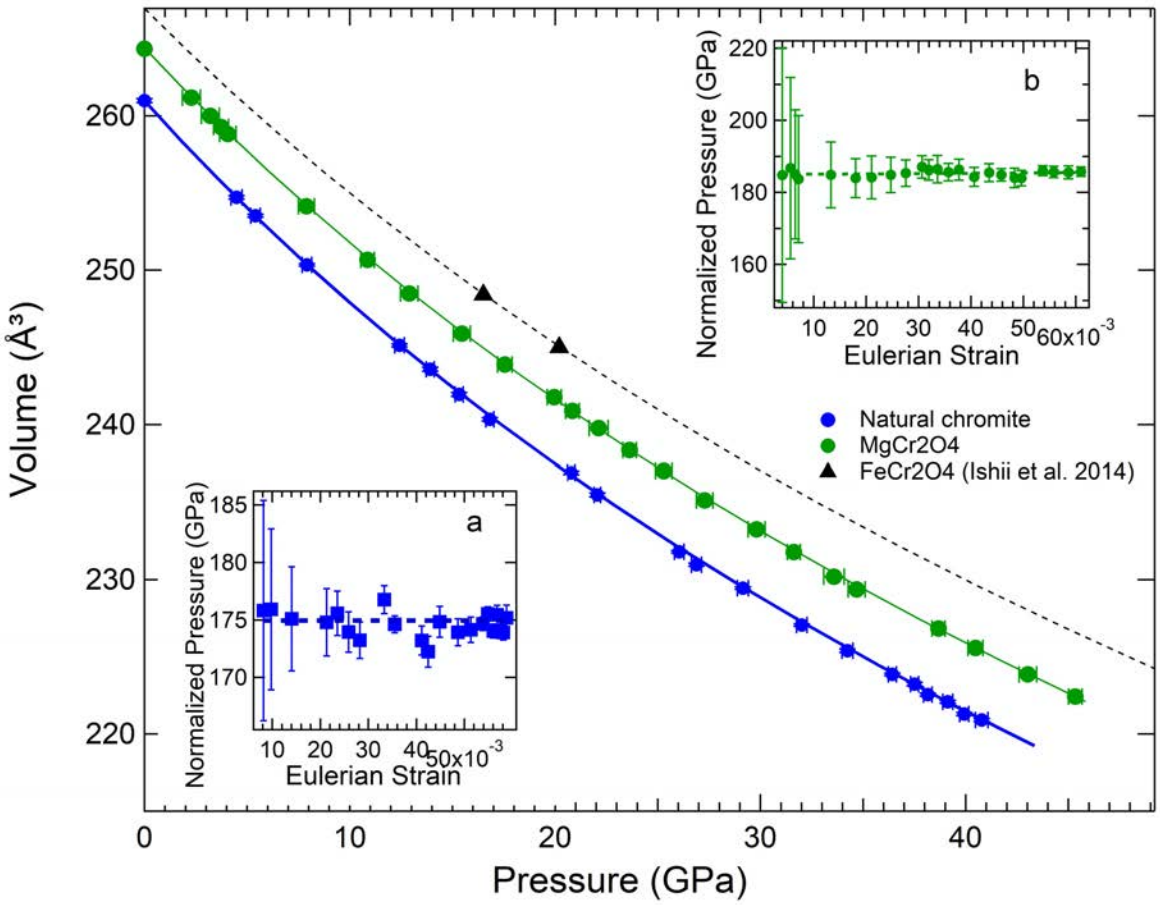

Figure 3: Volumes as a function of pressure for the CT phase of $MgCr_2O_4$, natural $(Mg,Fe)(Al,Cr)_2O_4$ and synthetic $FeCr_2O_4$. (i) Natural $(Mg,Fe)(Al,Cr)_2O_4$: ambient volume V_0 = 261(1) Å^3, Bulk Modulus K_0 = 175.4(2) GPa, and K_0' = 4; (ii) $MgCr_2O_4$: V_0 = 264.4(8) Å^3, K_0 = 185.4(4) GPa, and K_0' = 4; and (iii) synthetic $FeCr_2O_4$ (Ishii et al. 2014) : V_0 = 266.95 Å^3, K_0 = 199 GPa, and K_0' = 4. Pressure derivative of the isothermal bulk modulus (K_0') was determined using normalized pressure and Eulerian Strain relationship for both CT phase of natural $(Mg,Fe)(Al,Cr)_2O_4$ (lower left inset a) and $MgCr_2O_4$ (upper right inset b).

This is the peer-reviewed, final accepted version for American Mineralogist, published by the Mineralogical Society of America.
The published version is subject to change. Cite as Authors (Year) Title. American Mineralogist, in press.
DOI: https://doi.org/10.2138/am-2021-7853. http://www.minsocam.org/

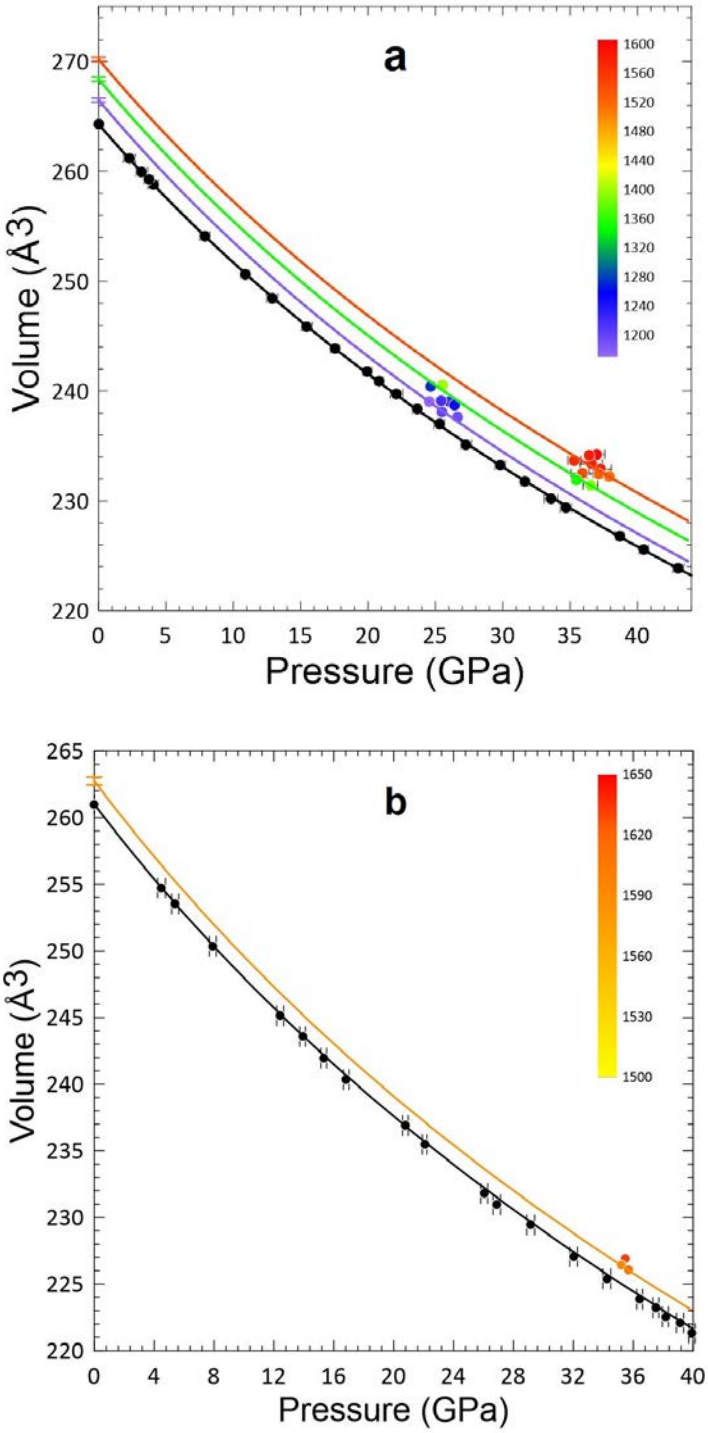

Figure 4: Pressure-volume-temperature data and isotherms of 1200, 1400 and 1550 K for the CT phase of $MgCr_2O_4$ (a) and 1600 K for the CT phase of natural $(Mg,Fe)(Al,Cr)_2O_4$ (b). Black circles are room-temperature data and color symbols are high-temperature data.

This is the peer-reviewed, final accepted version for American Mineralogist, published by the Mineralogical Society of America.
The published version is subject to change. Cite as Authors (Year) Title. American Mineralogist, in press.
DOI: https://doi.org/10.2138/am-2021-7853. http://www.minsocam.org/

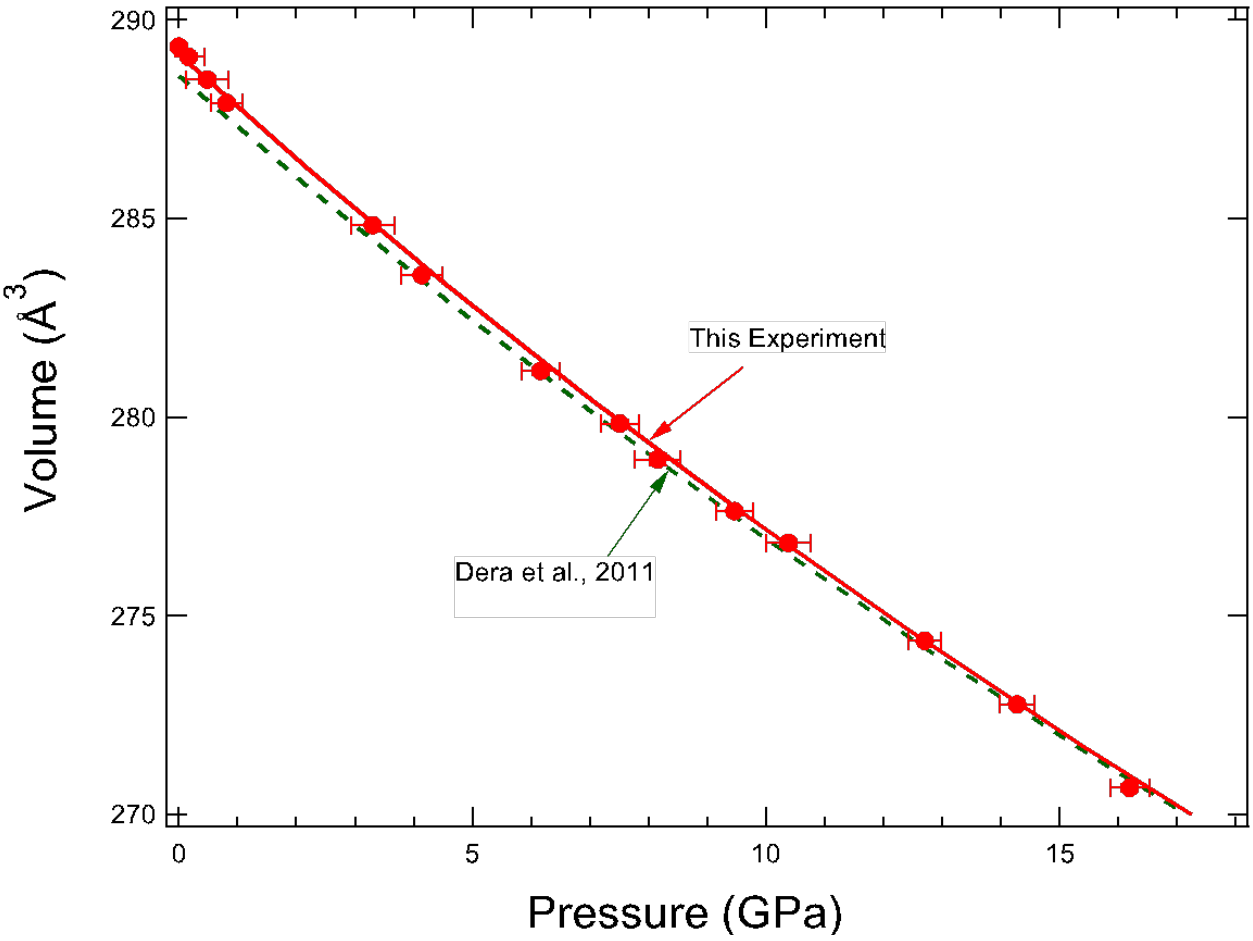

Figure 5: Comparison of the Birch-Murnaghan EOS fitting curve of Cr_2O_3 between this study and Dera et al. (2011).

This is the peer-reviewed, final accepted version for American Mineralogist, published by the Mineralogical Society of America.
The published version is subject to change. Cite as Authors (Year) Title. American Mineralogist, in press.
DOI: https://doi.org/10.2138/am-2021-7853. http://www.minsocam.org/

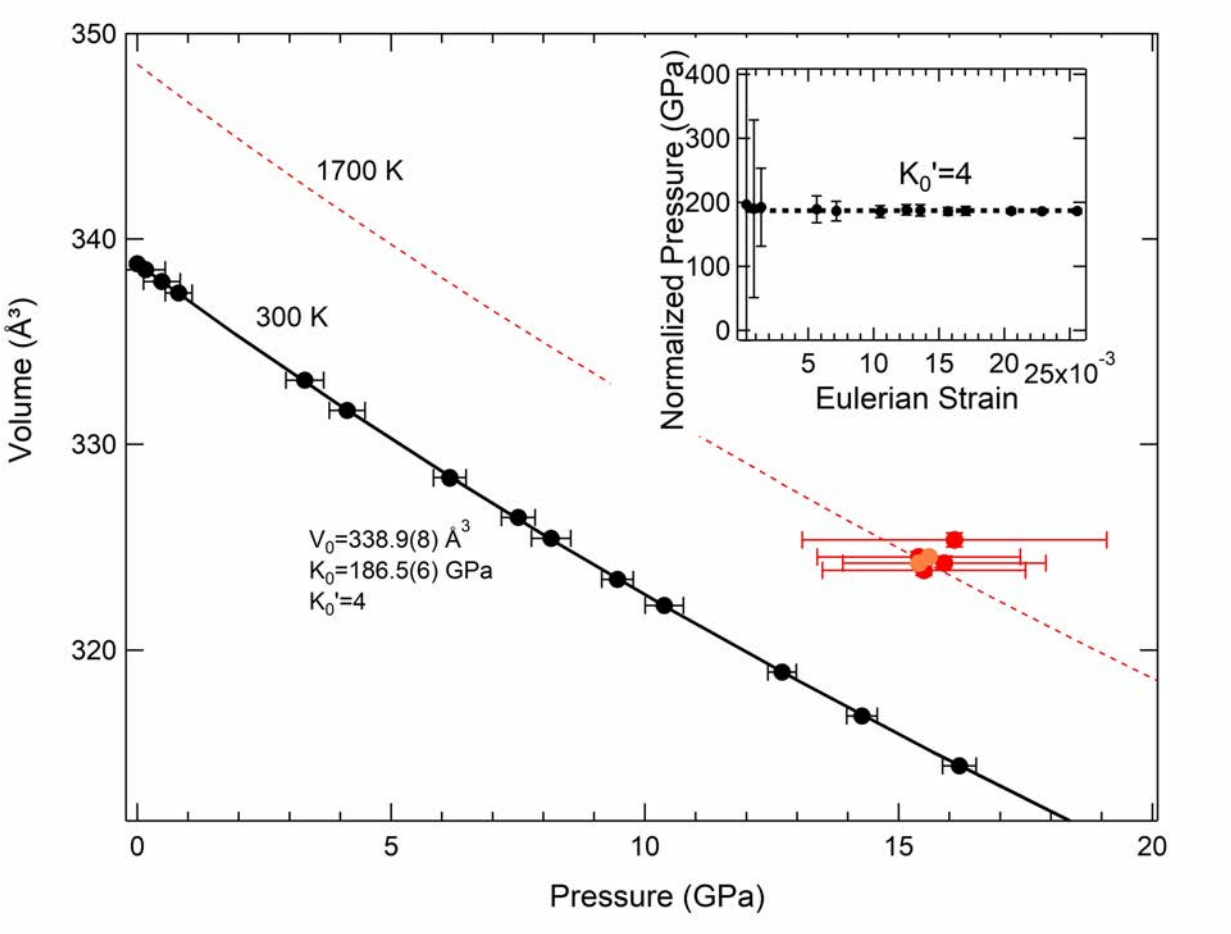

Figure 6: Pressure-volume-temperature data of modified Ludwigite-type $Mg_2Cr_2O_5$ phase. The inset shows a linear relationship of normalized pressure and Eulerian strain for modified Ludwigite-type $Mg_2Cr_2O_5$ phase. Black circles are data from room temperature, orange circles are data from 1590 K and red circles are data from 1700-1730 K.

This is the peer-reviewed, final accepted version for American Mineralogist, published by the Mineralogical Society of America.
The published version is subject to change. Cite as Authors (Year) Title. American Mineralogist, in press.
DOI: https://doi.org/10.2138/am-2021-7853. http://www.minsocam.org/

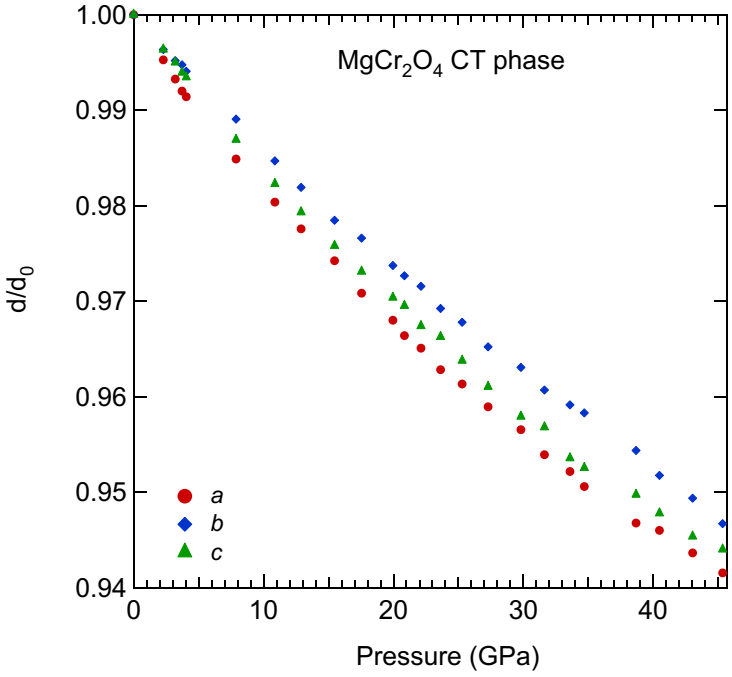

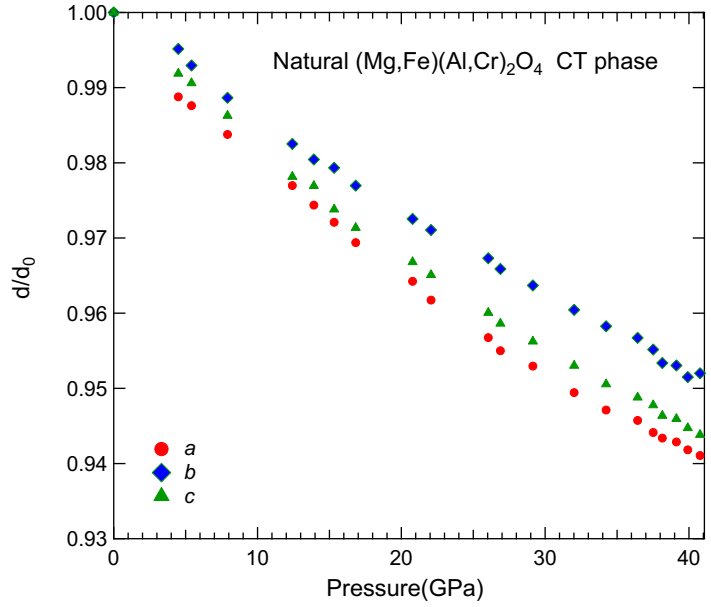

This is the peer-reviewed, final accepted version for American Mineralogist, published by the Mineralogical Society of America.
The published version is subject to change. Cite as Authors (Year) Title. American Mineralogist, in press.
DOI: https://doi.org/10.2138/am-2021-7853. http://www.minsocam.org/

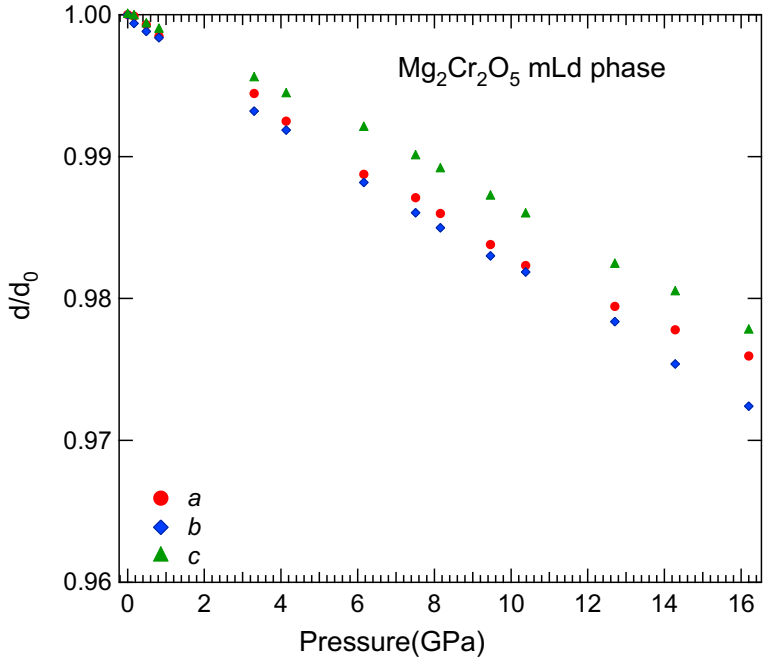

Figure 7: Axial compressibility of (top) the CT phase of $MgCr_2O_4$, (middle) the CT phase of natural $(Mg,Fe)(Al,Cr)_2O_4$ and (bottom) the modified Ludwigite-type $Mg_2Cr_2O_5$ at high pressures. Three phases all show weak anisotropic behavior.

This is the peer-reviewed, final accepted version for American Mineralogist, published by the Mineralogical Society of America.
The published version is subject to change. Cite as Authors (Year) Title. American Mineralogist, in press.
DOI: https://doi.org/10.2138/am-2021-7853. http://www.minsocam.org/

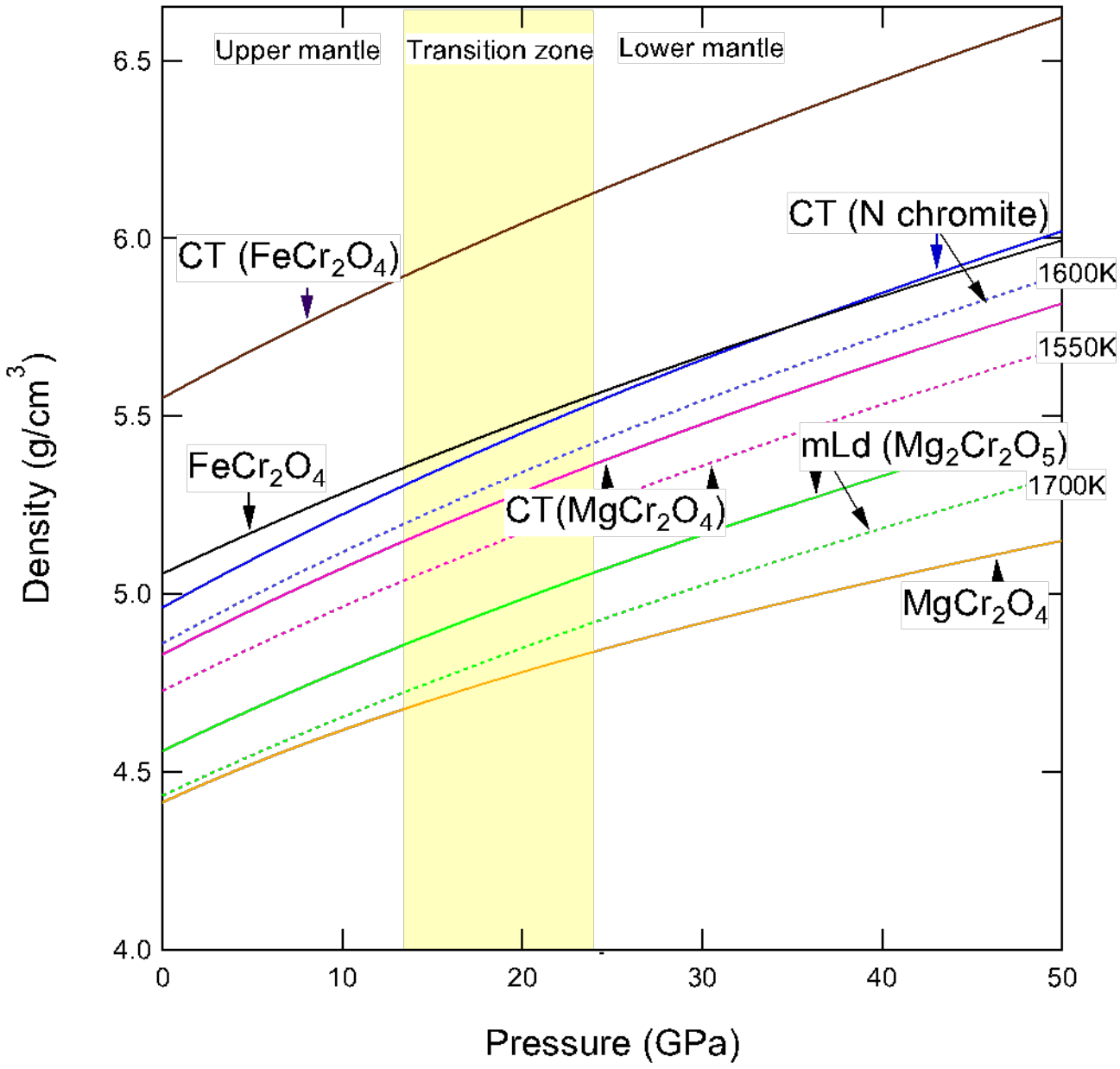

Figure 8: Density as a function of pressure for $MgCr_2O_4$, $FeCr_2O_4$, mLd-type $Mg_2Cr_2O_5$, CT phase of $MgCr_2O_4$, CT phase of $FeCr_2O_4$ and CT phase of natural $(Mg,Fe)(Al,Cr)_2O_4$. N chromite stands for natural $(Mg,Fe)(Al,Cr)_2O_4$. Solid curves are data from room temperature and dashed curves are data from high temperatures.

This is the peer-reviewed, final accepted version for American Mineralogist, published by the Mineralogical Society of America.
The published version is subject to change. Cite as Authors (Year) Title. American Mineralogist, in press.
DOI: https://doi.org/10.2138/am-2021-7853. http://www.minsocam.org/

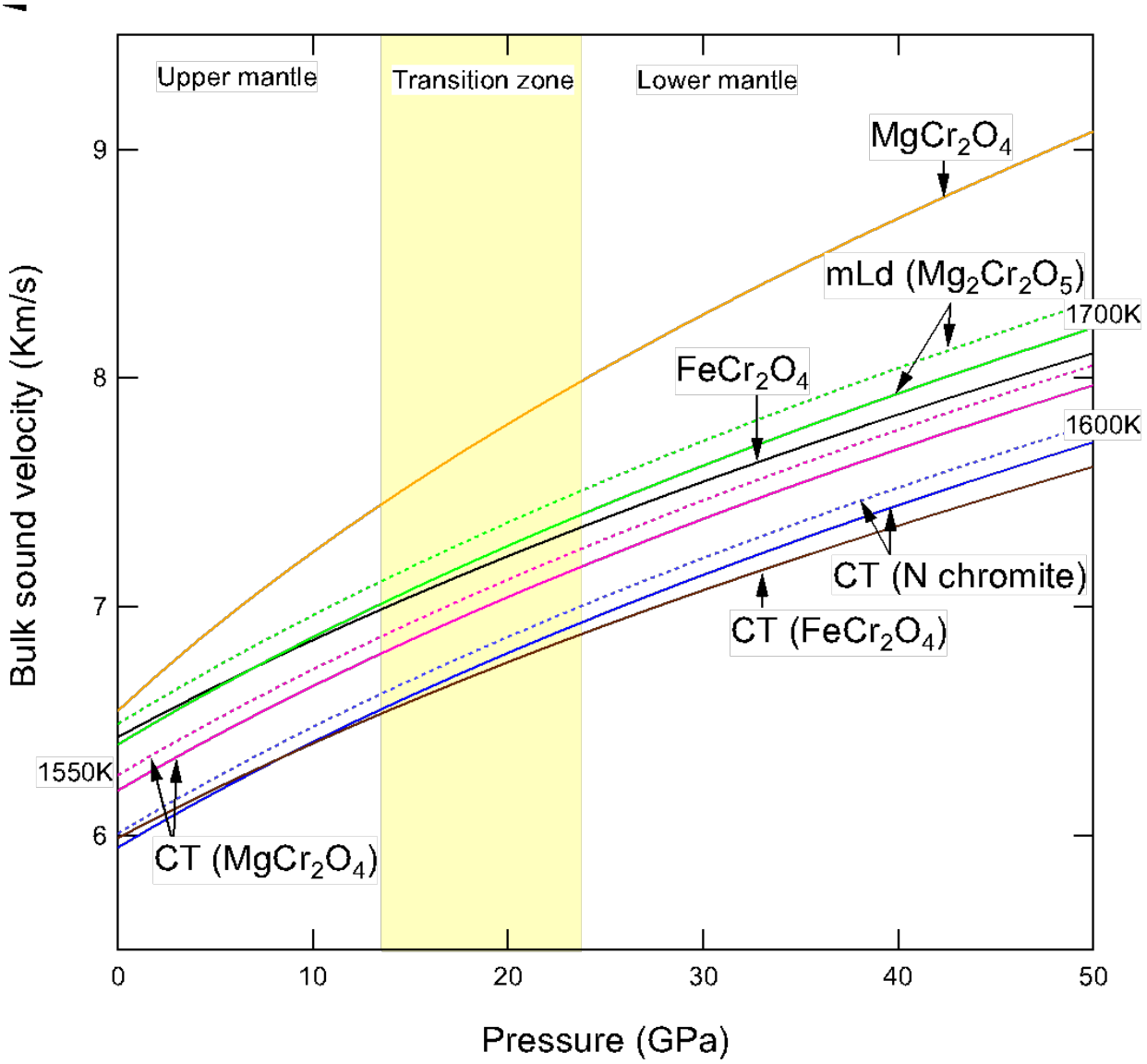

Figure 9: Bulk sound velocity as a function of pressure for $MgCr_2O_4$, $FeCr_2O_4$, mLd-type $Mg_2Cr_2O_5$, CT phase of $MgCr_2O_4$, CT phase of $FeCr_2O_4$ and CT phase of natural $(Mg,Fe)(Al,Cr)_2O_4$. N chromite stands for natural $(Mg,Fe)(Al,Cr)_2O_4$. Solid curves are data from room temperature and dashed curves are data from high temperatures.